Geol. Mag. **139** (*3*), *2002, pp. 343–359. © 2002 Cambridge University Press*
DOI: 10.1017/S0016756802006489 *Printed in the United Kingdom*

Palaeostress analysis of Tertiary post-collisional structures in the Western Pontides, northern Turkey

GÜRSEL SUNAL* & OKAN TÜYSÜZ†

*Istanbul Technical University, Faculty of Mines, Geology Department, 80626, Maslak, Istanbul, Turkey
†Istanbul Technical University, Eurasia Institute of Earth Sciences, 80626, Maslak, Istanbul, Turkey

(*Received* 25 July 2001; *accepted* 14 January 2002)

Abstract – Fingerprints of the opening of the Western Black Sea Basin and collision of Pontides and Sakarya Continent along the Intra-Pontide suture can be traced in the area between Cide (Kastamonu) and Kurucaşile (Bartın) in northern Turkey, along the southern coast of the Black Sea. The Western Black Sea Basin is an oceanic basin opened as a back-arc basin of the northward-subducting Intra-Pontide Ocean. Basement units related to this opening are represented by Lower Cretaceous and older units. The first arc magmatism related to this subduction began during Turonian times. Coeval with this magmatism, back-arc extension affected the region and caused development of horst-graben topography. This extensional period resulted in the break-up of continental crust and the oceanic spreading in the Western Black Sea Basin during Late Santonian times. During the Late Campanian–Early Maastrichtian period, the Sakarya Continent and Pontides collided and arc magmatism on the Pontides ended. After this collision, the Western Pontides thickened, imbricated and developed a mainly N-vergent foreland fold and thrust belt character since Late Eocene–Oligocene times. The palaeostress directions calculated from thrust faults of this foreland fold and thrust belt are 4.6°/156.6° for σ1, 6.4°/66.1° for σ2, and 83.2°/261.9° for σ3. The nature of the imbrication indicates that it was a northward prograding foreland system connected to a floor thrust (detachment) fault at the bottom. Field observations on curved slickenfibres support the theory that the thrust faults of this imbricated structure have transformed to oblique thrusts and strike-slip faults over time.

Keywords: fold and thrust belts, Pontic Mountains, Turkey.

1. Introduction

The study area is located on the southern margin of the Western Black Sea Basin, on a small continental fragment known as either the Istanbul Zone (Okay, Şengör & Görür, 1994) or the Western Pontides (Şengör & Yılmaz, 1981) (Fig. 1). This fragment is delimited by the Intra-Pontide Suture in the south and by the Western Black Sea Basin to the north. A Palaeozoic sedimentary unit and underlying high-grade metamorphic association form the visible basement of the Western Pontides (Abdüsselamoğlu, 1977; Görür *et al.* 1997). Overlying are Triassic red beds and Dogger marine clastics (Figs 1, 2). In contrast to the Western Pontides, Triassic units in the Central and Eastern Pontides are mainly polyphase metamorphosed and are oceanic in origin (Tüysüz, 1990).

Although a Lias age and a back-arc mechanism of opening have been proposed for the Intra-Pontide Ocean in the northernmost branch of Neotethys (Şengör & Yılmaz, 1981; Görür *et al.* 1983), its opening time and mechanism is still a matter of debate. Late Jurassic platform carbonates deposited on the Western Pontides have been interpreted as south-facing passive continental margin sediments (Şengör & Yılmaz, 1981; Görür, 1988; Tüysüz *et al.* 1990; Görür *et al.* 1993; Tüysüz, 1993; Okay, Şengör & Görür, 1994). Lower Cretaceous sediments transgressively overlie the passive margin sediments made up of mainly siliciclastic turbidites with debris-flow horizons and blocks from the underlying units. Although these chaotic clastics have been regarded as syn-rift deposits of the Western Black Sea back-arc basin by previous authors (Görür, 1988; Görür *et al*. 1993), recent studies indicated that a magmatic arc was not developed on the Western Pontides until the Turonian age (Tüysüz, Sunal, & Kirici, unpub. Turkish Petroleum Company Report, 1997; Tüysüz, 1999). On the other hand, a normal faulting period was associated with the extensive Turonian volcanism. In the light of these data, Tüysüz, Sunal, & Kirici (unpub. Turkish Petroleum Company Report, 1997) and Tüysüz (1999) proposed that the main opening phase of the Western Black Sea Basin was during Turonian times.

During Late Campanian–Maastrichtian times, volcanic processes ended and the southern part of area started to uplift, most probably due to the continental collision between the Pontides and Sakarya Continent to the south (Okay & Tüysüz, 1999; Okay, Tansel & Tüysüz, 2001) (Fig. 1). After that time, the Pontides

* Present address: Universität Tübingen, Institut für Mineralogie, Petrologie und Geochemie, Wilhelmstrasse 56, D-72074 Tübingen, Germany
† Author for correspondence: tuysuz@itu.edu.tr

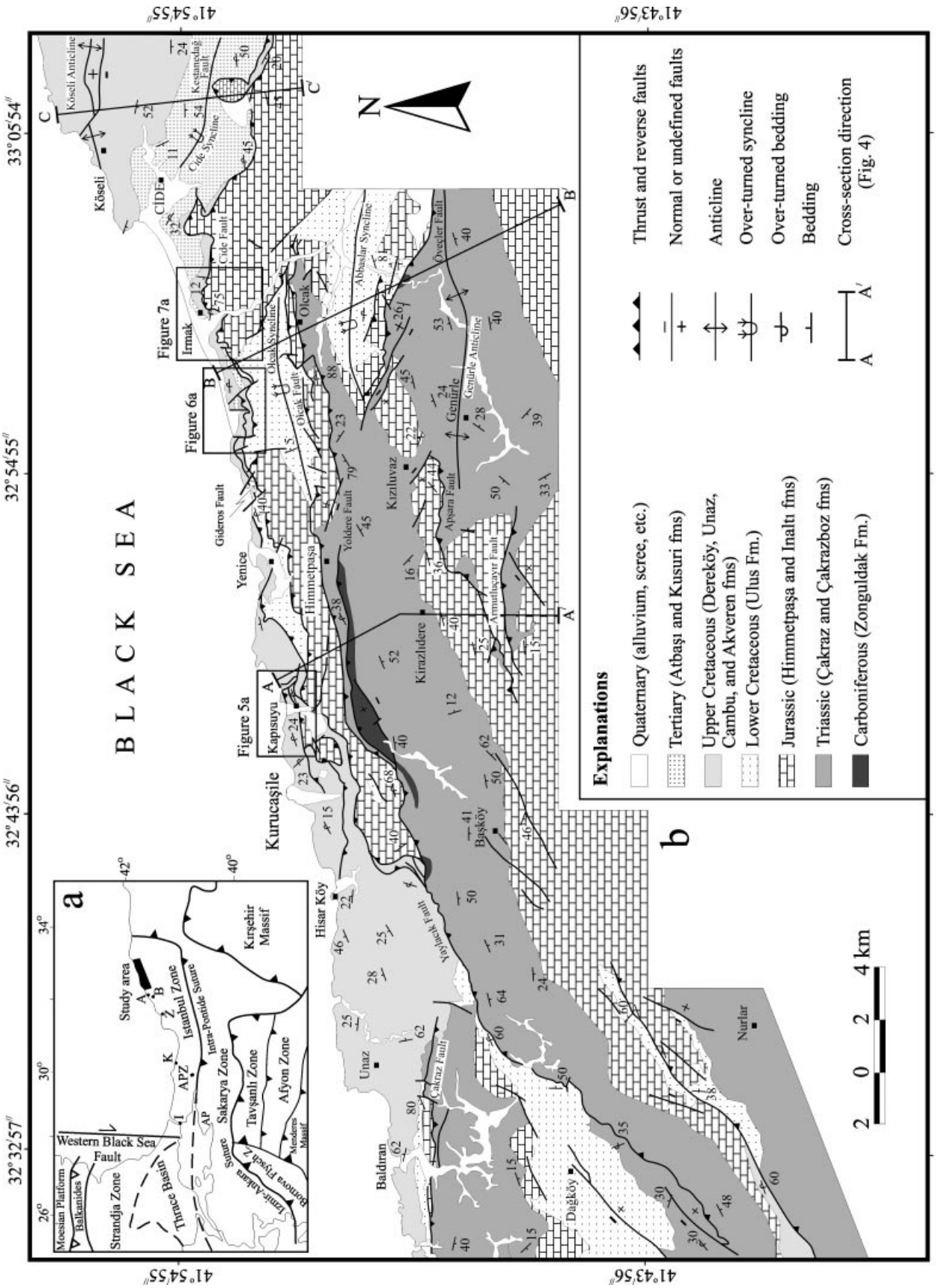

Figure 1. (a) Location and tectonic map of the study area (AP – Armutlu Peninsula, Z – Zonguldak, I – Istanbul, B – Bartın, A – Amasra, APZ – Adapazarı, K – Karasu), (b) Geological map of the study area.

https://doi.org/10.1017/S0016756802006489 Published online by Cambridge University Press

thickened, elevated, folded and imbricated due to a post-collisional compressional regime. According to Şengör (1995) this fold and thrust system developed over a detachment surface within the Lower Cretaceous units. The goal of this paper is to describe the nature of this fold and thrust belt for the first time, in the light of detailed geological mapping and structural measurements of kinematic indicators.

2. Stratigraphy

Stratigraphy of the study area can be divided into three parts: Lower Cretaceous and older units represent the basement with respect to the opening of the Western Black Sea Basin (Görür, 1997; Görür & Tüysüz, 1997; Görür *et al.* 1995) (Fig. 2); syn-rift sediments are known as the Dereköy Formation, which is Turonian in age; post-rift sediments consist of Upper Cretaceous to Eocene volcanics, clastics and carbonates (Figs 1, 2).

2.a. Basement units

The oldest visible unit of the study area, the Zonguldak Formation (Fig. 2), consists of river, swamp and delta clastic sediments rich in hard coal. Plant fossils indicating Namurian to Westphalian A, B and C have been described from these sediments (Akyol *et al*. 1974; Akman, 1992; Canca, 1994). In the neighbouring regions the Palaeozoic sequence continues downward from the Carboniferous to the Ordovician and rests unconformably on a high-grade metamorphic basement (Görür *et al.* 1997).

The Çakraz Formation, which is made up of braided river deposits at the base and meandering river and flood plain deposits at the top, unconformably overlies the Zonguldak Formation (Figs 1, 2). The Çakraz Formation shows a transitional contact with the overlying Upper Triassic Çakrazboz Formation (Rutherford *et al.*, unpub. BP Exploration report, 1992; Alişan & Derman, 1995), suggesting a Permo-Triassic age. The Çakrazboz Formation comprises lacustrine limestones, marls and mudstones with varve structures (Alişan & Derman, 1995).

The Middle Jurassic Himmetpaşa Formation unconformably overlies Triassic and Carboniferous units (Akyol *et al.* 1974; Alişan & Derman, 1995; Tüysüz, 1999) (Fig. 2). It begins with coal-bearing, terrestrial sediments at the base and grades upwards into shallow to deep marine turbiditic clastics. The uppermost part of the succession is represented again by shallow marine clastics. Ammonites, gastropods and palynomorphs indicate a Dogger age for the Himmetpaşa Formation (Derman, Alişan & Özçelik, 1995).

The İnaltı Formation (Ketin & Gümüş, unpub. Turkish Petroleum Company Report, 1963) disconformably overlies the Himmetpaşa Formation. It is represented by platform-type neritic carbonates, which are Late Jurassic in age (Derman, Alişan & Özçelik, 1995; Tüysüz, Sunal & Kirici, unpub. Turkish Petroleum Company Report, 1997) (Fig. 2). The Inaltı Formation is the product of a Mesozoic transgression covering the whole of the Pontides (Şengör & Yılmaz, 1981; Görür, 1988; Tüysüz *et al.* 1990; Görür *et al.* 1993; Tüysüz, 1993).

The Ulus Formation is a thick marine clastic unit resting unconformably on the Inaltı Formation and older units (Figs 1, 2). It starts with beach sandstones and some local fanglomerates at the base and grades upward into turbiditic siliciclastics. Within this unit, debris-flows, large blocks of older units and some hemipelagic mudstones can be identified. According to Görür (1997), the Ulus Formation represents the syn-rift deposits of the Western Black Sea Basin. Recent studies showed that the Ulus Formation displays deeper marine conditions towards the south and southeast. Palaeocurrent measurements also indicate that the Ulus Formation was fed from the north. In the light of these data, Tüysüz (1999) argued that the Ulus Basin opened as a separate basin. If the Western Black Sea Basin was also opening at the same time in the north as claimed by the previous authors, an archipelago separated both basins.

2.b. Syn-rift units

The Ulus Formation is unconformably overlain by the Dereköy Formation of Turonian age (Figs 1, 2). The Dereköy Formation comprises the first magmatic rocks of the Western Pontides. These magmatic rocks were represented by thick basaltic and andesitic lava and their pyroclastics alternating with shallow and/or deep marine carbonates and clastics. Debris-flows, blocks and submarine slope-waste deposits occur within this unit (Tüysüz, Sunal & Kirici, unpub. Turkish Petroleum Company Report, 1997; G. Sunal, unpub. M.Sc. thesis, Istanbul Technical Univ., 1998) (Fig. 2). In addition to these fault-controlled deposits, the Dereköy Formation displays rapid changes in thickness and in environmental properties that have been interpreted as indicators of normal faulting during deposition (Tüysüz, Sunal & Kirici, unpub. Turkish Petroleum Company Report, 1997; Tüysüz, 1999; Tüysüz, Keskin & Sunal, 1999). In light of these data, Tüysüz (1999) concluded that this formation represents syn-rift deposits of the Western Black Sea back-arc basin.

2.c. Post-rift units

The post-rift units start with a thin Santonian pelagic limestone, the Unaz Formation. This formation displays different contact relations with the underlying formations due to horst and graben topography, which developed during the deposition of the Dereköy

https://doi.org/10.1017/S0016756802006489 Published online by Cambridge University Press

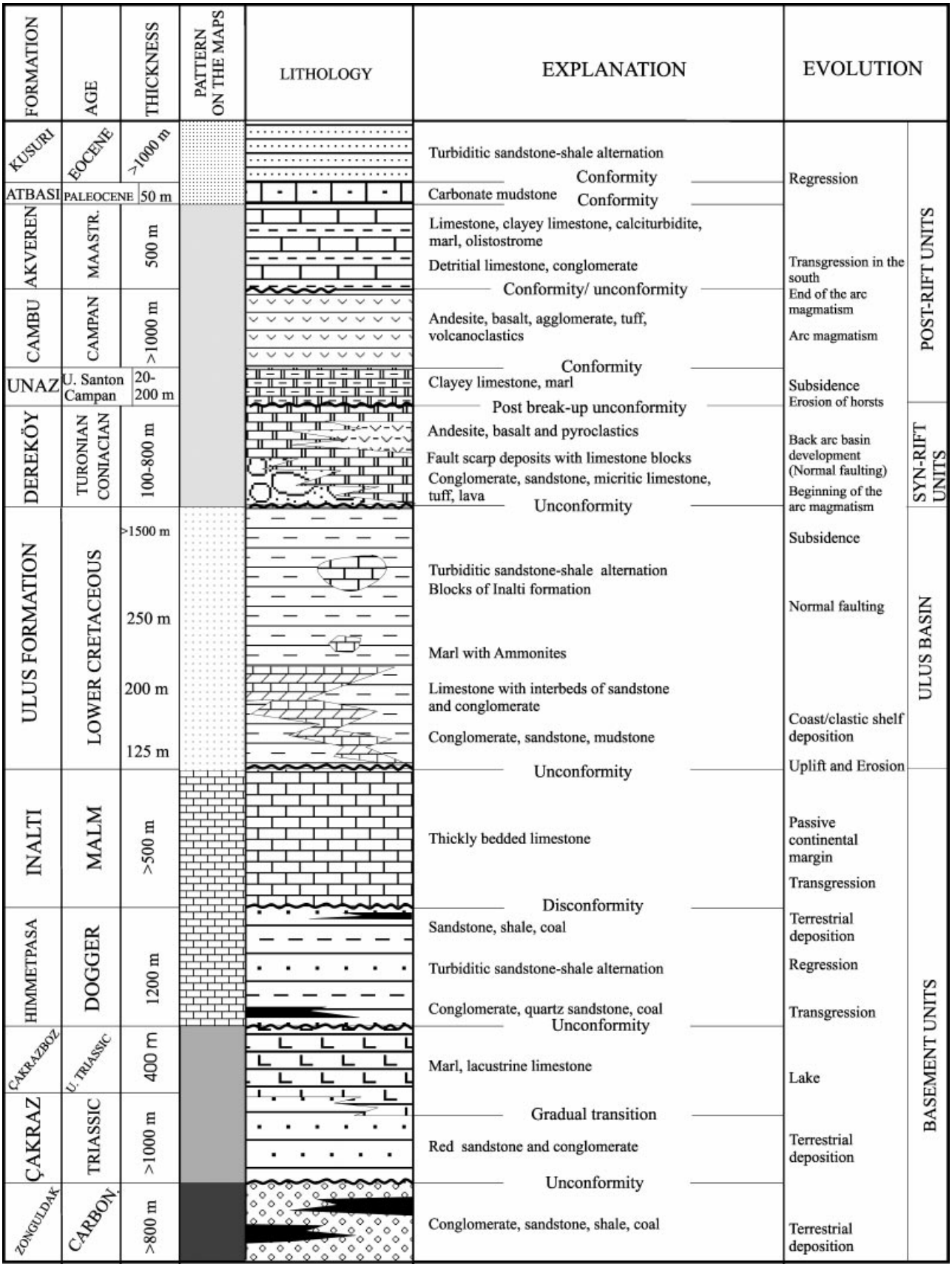

Figure 2. Generalized columnar stratigraphic section of the study area.

https://doi.org/10.1017/S0016756802006489 Published online by Cambridge University Press

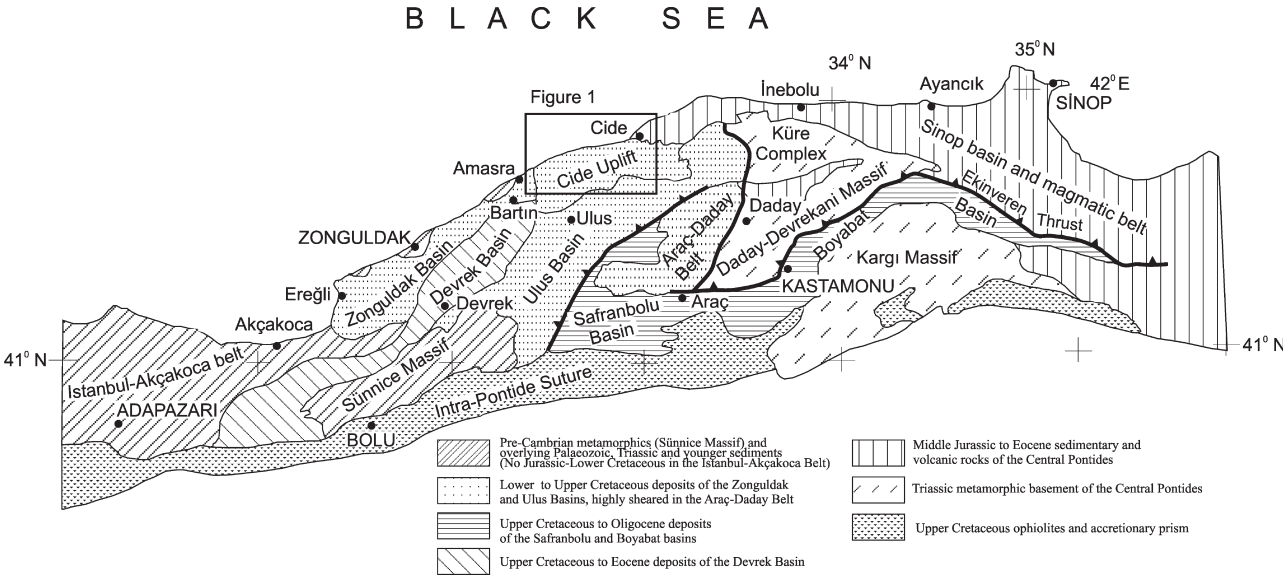

Figure 3. Main tectonostratigraphic features of the Western Pontides (after Tüysüz, 1999).

Formation. It unconformably overlies different basement rocks on the horsts and displays a transitional character with the syn-rift deposits within the grabens. This formation indicates a rapid subsidence at the beginning of the post-rift period and implies a drastic change in the sedimentation (Tüysüz, 1999). At that time volcanism stopped, all the region subsided and a wide transgression eliminated most of the terrigenous sediment sources, thus providing a suitable location for the deposition of the pelagic carbonates of the Unaz Formation. This change most probably indicates the onset of spreading in the Western Black Sea Basin during Santonian times (Görür *et al.* 1995).

A thick volcano-sedimentary succession, the Cambu Formation of Campanian age lies on the Unaz Formation (Fig. 2). This formation is seen all along the southern Black Sea region and it was produced by an extensive arc magmatism (Tüysüz, Sunal & Kirici, unpub. Turkish Petroleum Company Report, 1997; Tüysüz, Keskin & Sunal, 1999). There is general agreement that this arc was established as a result of the northward subduction of Neotethys beneath the Pontides.

The Akveren Formation of Maastrichtian age conformably overlies the Cambu Formation (Fig. 2). This formation, which marks the end of the arc magmatism, is mainly made up of calciturbidites, olistostromes and pelagic mudstones. Palaeocurrent measurements indicate that the Akveren Formation on the Black Sea coast was fed by an erosional area to the south (Tüysüz, Sunal & Kirici, unpub. Turkish Petroleum Company Report, 1997; G. Sunal, unpub. M.Sc. thesis, Istanbul Technical Univ., 1998). In contrast to the Black Sea coast, the Akveren Formation transgressively overlaps the basement units in the south, east of Bartın (Fig. 3) and in the Sünnice massif (Yiğitbaş, Elmas & Yılmaz, 1999). In these areas, the Akveren Formation starts with a basal conglomerate, which was locally deposited under the control of normal faults, and grades rapidly into Globotruncana-bearing pelagic micritic limestones. These data show that the southern parts of the study area uplifted soon after the deposition of the Cambu Formation, during the Late Campanian–Early Maastrichtian period, coeval with the end of volcanic activity. These two events most probably indicate termination of the Neotethyan Ocean by the collision of the Sakarya Continent and Western Pontides. This idea was also supported by data from the Central Pontides (Tüysüz, 1993; Tüysüz *et al.* 1995) and from the Armutlu Peninsula (Fig. 1).

The Akveren Formation gradually passes upward to pelagic mudstones and marls of the Paleocene Atbaşı Formation (Ketin & Gümüş, unpub. Turkish Petroleum Company Report, 1963), and siliciclastic turbidites of the Eocene Kusuri Formation (Figs 1, 2). The Kusuri Formation shows a regressive development and passes into shallow marine marls in the uppermost parts. Its thickness reaches up to 3500 m in the Devrek Basin in the south (Tüysüz, 1999) and up to a few kilometres in the southern Black Sea margin (Finetti *et al.* 1988) (Fig. 3).

3. Structural features of the study area

The study area is a N-vergent fold and thrust belt characterized by an imbricate structure (thin-skinned structures) (Figs 3, 4). Thrust (reverse) faults, folds and related small-scale structures such as cleavage and lineation are the main structural features (Figs 4–7).

https://doi.org/10.1017/S0016756802006489 Published online by Cambridge University Press

3.a. Faults

3.a.1. Thrust (reverse) faults

Thrust faults (the term 'thrust' will be used for all reverse faults, regardless of dip angle) in the investigated area are approximately parallel to the Black Sea shore. They can be divided into three belts (Figs 1, 4). Along the southernmost belt (Armutluçayır, Apşara and Malyas faults), the Zonguldak and Çakraz formations are thrust over the Inaltı and Ulus formations. Dips of the faults are generally steeper than 70° to the south. In this belt, units younger than Lower Cretaceous do not appear and thrusting is the dominant style of faulting. Moreover, some of the faults are displaced by N-trending transfer faults (Figs 1, 6a, 7a).

Within the intermediate fault belt (Olcak, Yoldere, Pelitova and Yaylacık faults), the fault planes dip more gently (50°–75°) compared to those of the southern fault belt. Similar to the southernmost belt, the faults in the intermediate belt emplaced the Zonguldak and Çakraz formations thrust over the Inaltı and Ulus formations (Fig. 1).

The northernmost fault belt is composed of the Kestanedağ, Cide and Gideros faults and extends along the southern shore of the Black Sea (Fig. 1). Dips of the fault planes in this belt range between 0° and 50° to the south (Figs 1, 4). Faulting in the northernmost belt mainly involves fine-grained syn- and post-rift deposits and hence meso-scale (outcrop scale) structures best developed within this belt, and they have been investigated in detail (Figs 5–7). Fault zones defined by large-scale thrusts are represented by incohesive cataclasites and gouges up to 6 m thick. Interaction between competent units produced mainly incohesive cataclasites. These cataclasites show secondary shear fractures and are mainly cemented by precipitation from carbonate solutions. Fault gouges are generated generally between competent–incompetent, and incompetent units. Foliation and secondary shear planes are well developed.

Dip angles of the faults that are responsible for the imbricated structure of the northernmost area are between 0°–50° in the north but they become steeper toward the south, and thrust faults turn into high angle reverse faults (Fig. 4). The incremental increase in dip angle of the fault planes towards the south indicates that the system has a leading imbricated structure and that subsequent underplating thrust sheets increase the dip angle of the pre-existing fault planes within the previous or trailing thrust sheets (Fig. 8; Mitra, 1986). Due to a continuous underplating system, faults that were originally low-angle thrusts become steeper and evolve to reverse faults over time (Figs 4, 8). Moreover, it is thought that the dip of the reverse faults decreases with depth in the southern region. The meso-scale thrust faults that have the same structural style support this idea (Figs 4–7).

3.a.2. Transfer faults

In the study area, there are faults trending approximately N–S, which have developed mainly where massive limestones of the Inaltı Formation form the hanging wall. These faults trend NNW in the northern belt and NNE in others. Lateral offsets measured in these faults are between 25–300 m (Figs 6a, 7a).

3.a.3. Normal faults

In the study area, there are no large-scale normal faults except one around Himmetpaşa village (Fig. 1). Instead, there are mostly small-scale normal faults that are related to the folding and shearing processes which developed during thrust faulting (Figs 5, 6). The single mappable normal fault at 1 : 25 000 scale has been observed around the village of Himmetpaşa. Slip on this normal fault occurs within the overturned limb of an overturned anticline. The small-scale normal faults can be observed in the structural sections (Figs 5–7).

3.b. Folds

Folds observed in the study area are overturned anticlines and synclines that have approximately S-dipping axial planes and the E–W-directed hinges indicating north vergence. Directions of the hinge lines are mostly parallel to the fault traces (Fig. 1). Macro-scale (first ordered: Nickelsen, 1963; Mitra, 1986) folds are ramp anticlines and synclines (fault-bend folds: Suppe, 1983, and fault-propagation folds: Suppe & Medwedeff, 1984; Mitra, 1986, 1990; Suppe & Medwedeff, 1990) (Figs 4, 6, 8). Especially in the northern belt, these structures can easily be observed. In addition, imbricated forelimb thrusts developed on the frontal limbs of some meso-scale folds (second and third ordered structures: Nickelsen, 1963; Mitra, 1986). These types of folds were named 'hybrid folds' by Berger & Johnson (1980) (Figs 5b, 6b).

In the southern part of the study area, the Zonguldak and Çakraz formations are exposed in the axes of anticlines, such as the Genürle anticline, while the Ulus Formation is exposed in the axes of synclines, such as the Abbaslar and Malyas synclines (Figs 1, 4). In contrast to the south, Upper Cretaceous and younger units are exposed in both anticlines and synclines in the northern part of the study area (Fig. 4).

Folds in the area are asymmetric, semi-cylindrical, gently plunging, overturned, rarely recumbent, and commonly chevron type in the Ulus Formation. The interlimb angles of the folds are generally less than 50°.

3.c. Small-scale structures

Most of the observations on small-scale structures have been done in the Akveren Formation and in some parts of Atbaşı and Dereköy formations (Figs 5–7).

Small-scale folds show similar geometry to those of

https://doi.org/10.1017/S0016756802006489 Published online by Cambridge University Press

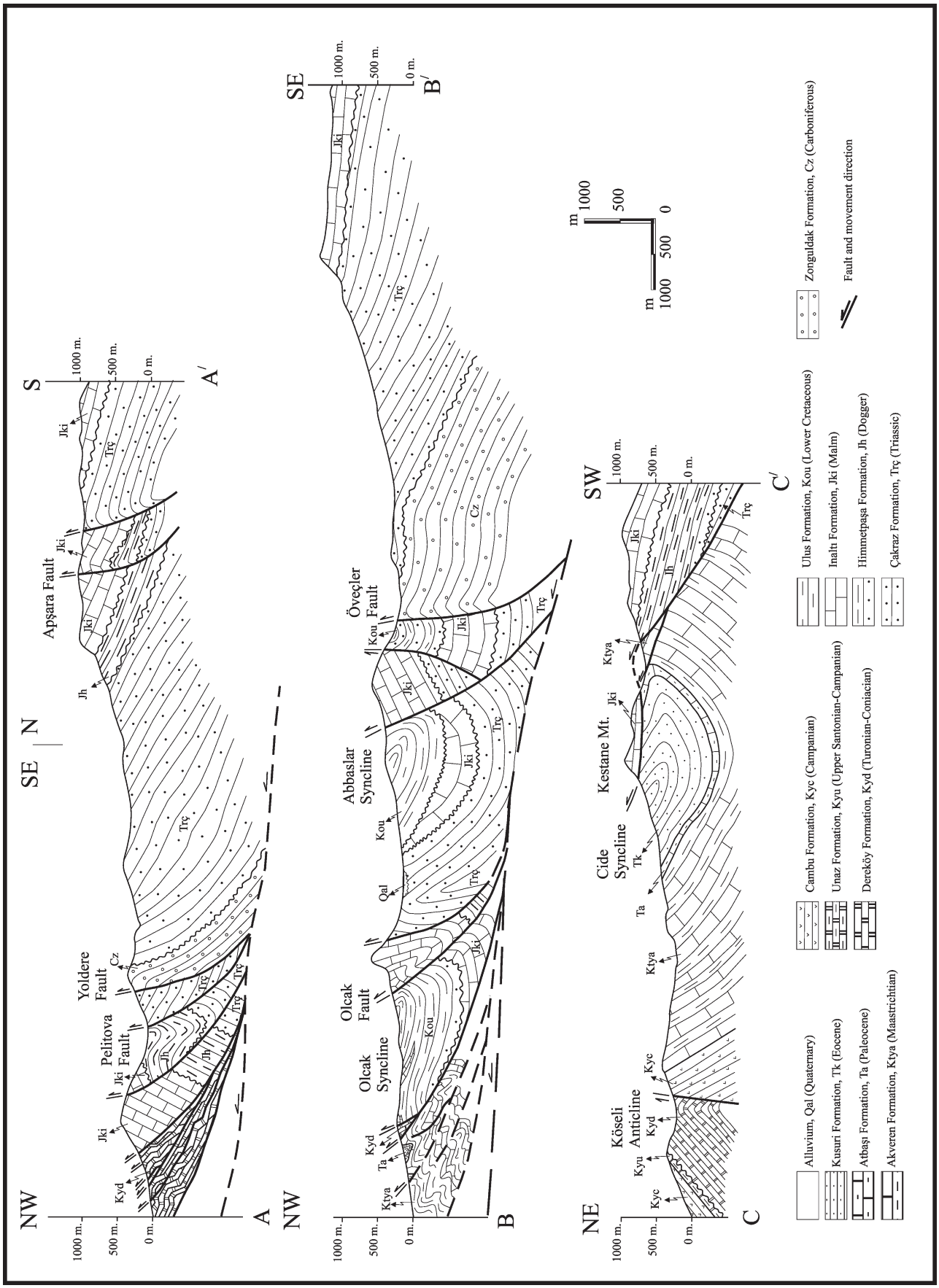

Figure 4. Geological cross-sections of the study area. See Figure 1 for locations of cross-sections.

https://doi.org/10.1017/S0016756802006489 Published online by Cambridge University Press

the macro-scale folds (Figs 5, 6). The average vergence direction of the folds that were measured in the Akveren Formation exposed on the footwall of the Gideros fault (northern belt) is N10°–20°W, and the strike of the axial planes is about N70°–80°E (Fig. 10a). Π poles indicate that the study area compressed roughly NNW–SSE (Fig. 9a). Poles to the reversed beds of the overturned folds are located in the northern area of the diagram.

Different lithologies that make up the Akveren Formation showed different behaviours under deformation (Fig. 5). Competent lithologies such as limestones, calciturbidites, conglomerates and clayey limestones exhibit brittle behaviour and show fracture cleavage, gouge and brittle faults (Figs 5–7). The incompetent lithologies such as marl and claystones were transported towards the core of the folds by small-scale dentritic faults (Passchier & Trouw, 1996). As a result, the limbs of the folds thinned and the core of the folds thickened (Fig. 5). Additionally, some small-scale strike-slip (except transfer faults), oblique thrust, and normal faults have been observed in structural sections (Figs 5–7). The surfaces of the small-scale faults are covered by up to 3 mm thick, syn-kinematic calcite fibres which indicate slickensides and corresponding slip lines. In the incompetent units, fault zones are represented by milled wall rocks and reveal pressure solution foliation with elements of S/C fabric. Syn-kinematic, en-echelon tension gaps were filled by carbonate material. In addition, centimetre-scale, asymmetric drag folds indicating sense of fault motion are present.

Cleavage has developed widely in the region studied. Fracture cleavage (disjunctive cleavage: Passchier & Trouw, 1996) in the competent lithologies and axial plane cleavage (slaty cleavage) in the less competent lithologies have been observed. In the contact between competent and less competent units, the different cleavages refract due to their rheological differences (Fig. 6). The axial plane cleavage is common especially in the Ulus Formation. Fracture cleavage planes have an angle to the axial planes of the folds due to rotation of cleavage planes under shearing and due to cleavage refraction (Fig. 6). The maximum density point on the π-diagram of cleavage planes is 36°/353° (Fig. 9c). A compression direction of N7°W can be derived from this maximum density point.

Structural sections in the study area represent the structural style of the whole region (Figs 5–7). Most of the faults are thrust faults with variable dip angles. In some places, they have a duplex or imbricated structure. In the duplex structure, flats (sole faults) use bedding surfaces, ramps (slopes) cut bedding surfaces, and slices (horses) are bounded by faults at both the bottom and top (B–B′ section in Fig. 4). Furthermore, in the imbricated structures, faults are connected to a floor thrust (detachment) at the bottom. Macro-structures in the study area were interpreted based on such meso-scaled faults and folds (Figs 4–7).

3.d. Timing of deformation

The compressional structures such as folds and thrusts described above affected all the Middle Eocene and older stratigraphic units in the Western Pontides, implying that the structures are younger than the Middle Eocene. As there are no Upper Eocene and younger rocks in the study area the upper age limit of the deformation cannot be constrained. However, data from the Central Pontides indicate that Oligocene sediments of the Boyabat Basin (Tüysüz, 1990, 1993, 1999) were also affected by similar contractional deformation, whereas Upper Miocene sediments in different parts of the Pontides are largely free from contractional deformation. This suggests that the main compressional deformation in the Western Black Sea region was between the Late Eocene and Early Miocene periods. This idea is supported by offshore seismic reflection studies (Finetti *et al.* 1988).

4. Palaeostress analysis

In this section, mainly thrust faults will be analysed, but other types of faults observed in the study area will be noted in Section 5. For the stress direction computation, we used a computer program written by Johannes (2000). Figure 11 shows each kind of fault observed in the study area, and corresponding striations and their palaeostress directions as computed by the method of *P*–*T* axes (Turner, 1953). In the *P*–*T* axes method, estimates of σ1 and σ3 axes are located in the movement plane 45° and 135° respectively, from the slip lineation using the sense of movement. The σ2 axis lies on the normal to the movement plane. Although this assumption is only valid for ideal homogeneous media, sometimes this method still yields meaningful results. Palaeostress directions resolved from the thrust faults given in Figure 10a reveal that σ1 is oriented at 156° with a plunge of about 5°, and σ3 is approximately vertical. σ2 is sub-horizontal like σ1, oriented at 66° with a plunge of about 6°.

We then analysed the same data manually, using the M-pole girdle solution method of Angelier (1979, 1984) to test the *P*–*T* method of Turner (1953). In contrast to Turner's method, the M-pole girdle method can be run for inhomogeneous media. Figure 11a shows M-planes and M-poles of thrust faults. The M-plane is the movement plane that is produced from the pole to fault plane and the corresponding striation (Arthaud, 1969). The M-pole density pattern and the girdle are given in Figure 11c. In this diagram the M-pole girdle contains σ1 and σ2 directions and the pole to M-pole girdle coincides with the σ3 direction. However, the exact positions of the σ1 and σ2 directions are not clear. With this method we can only determine the σ1–σ2 great circle (M-pole girdle) that is located around the prime. To solve this problem, we assume that if the σ2 is located on the fault surface, the intersection point of mean S- and N-dipping faults should be coincident with the σ2 point (Fig. 11b, data

https://doi.org/10.1017/S0016756802006489 Published online by Cambridge University Press

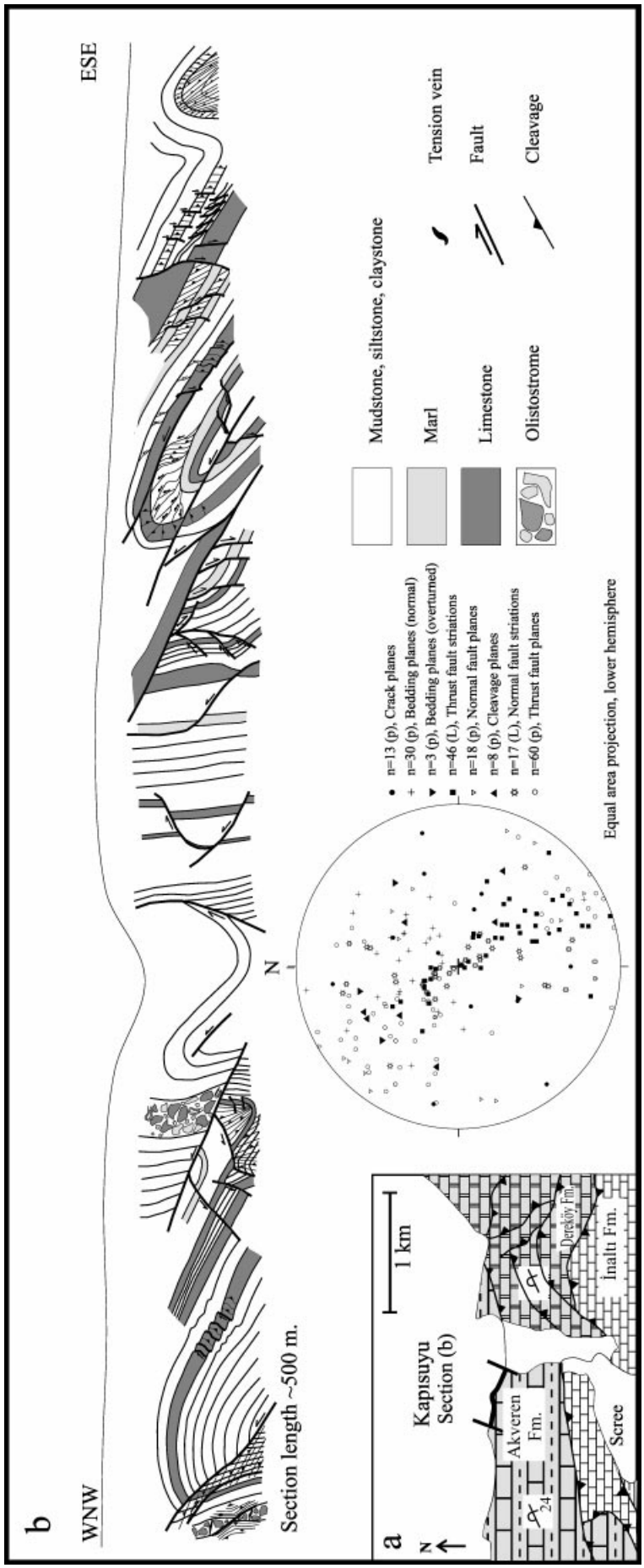

Figure 5. (a) Detailed location map of section presented in (b) (location is given in Fig. 1). (b) Structural cross-section of the Akveren Formation across the Kapısuyu beach.

https://doi.org/10.1017/S0016756802006489 Published online by Cambridge University Press

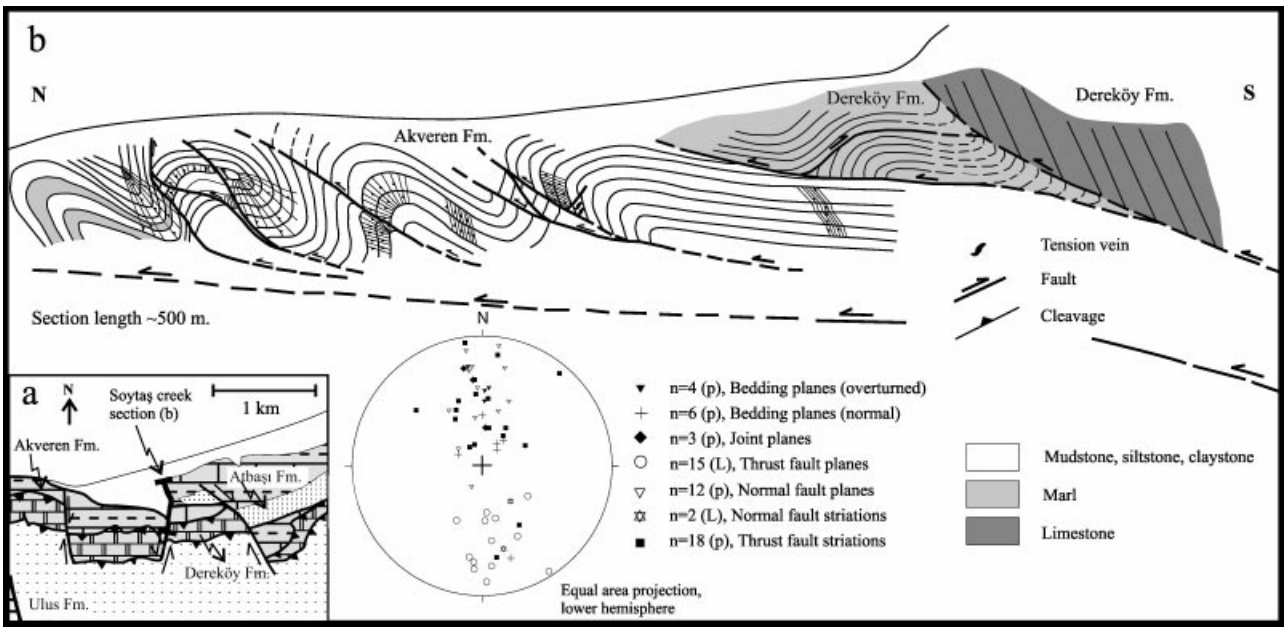

Figure 6. (a) Detailed location map of section presented in (b) (location is given in Fig. 1). (b) Structural cross-section along the Soytaş creek.

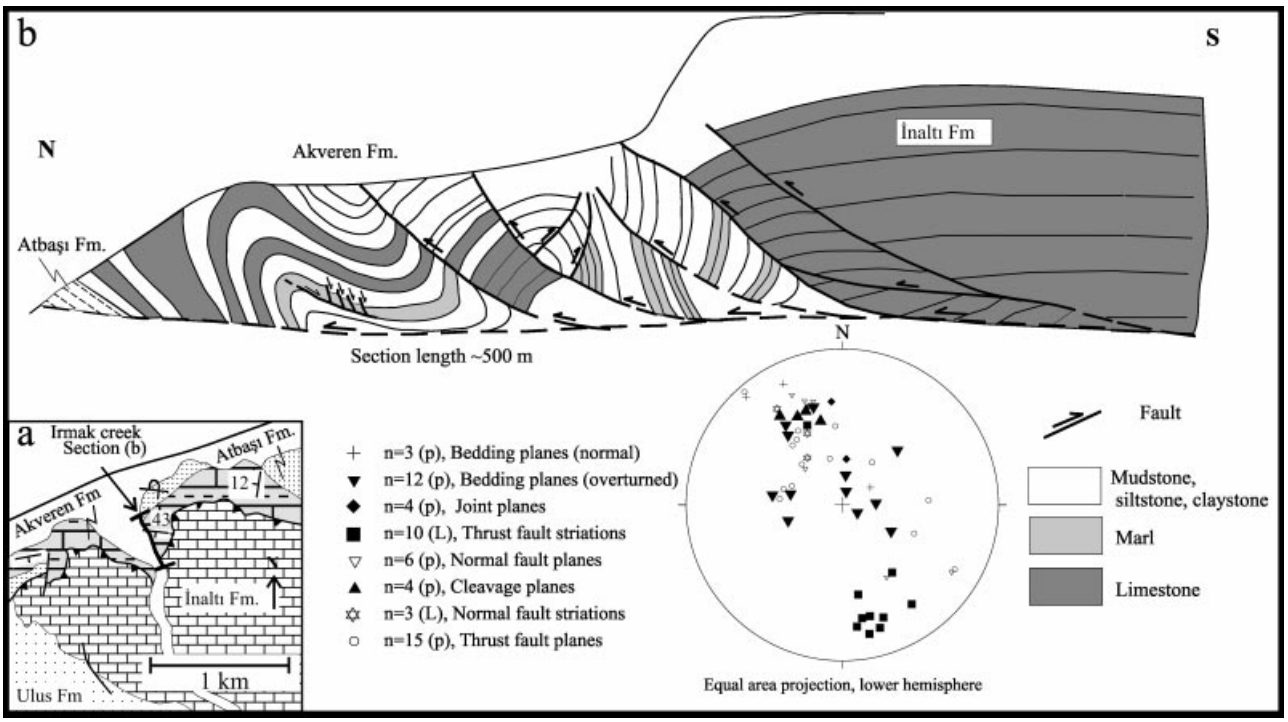

Figure 7. (a) Detailed location map of section presented in (b) (location is given in Fig. 1). (b) Structural cross-section along the Irmak creek.

used for all thrust faults given in Fig. 9f). Cross-cutting relations observed in the field indicate that both S- and N-dipping faults are conjugate in nature. In the light of this assumption, we placed mean S- and N-dipping thrust fault planes on the M-pole density diagram (Fig. 11c). σ2′ indicates this intersection point and is located approximately on the M-pole girdle (σ1–σ2 great circle in Fig. 11c). If our assumption is relevant it is easy to recognize the σ1′ that is indicated in both Figure 11b and 11c (normal to σ3 and σ2′ great circle).

We also analysed our data using right-dihedra and right-trihedra methods (Ramsey & Lisle, 2000) and determined that σ1 is sub-horizontal and directed NW–SE, and σ3 is approximately vertical.

When the results of M-pole girdle analysis are compared with the results obtained from the other methods, it can be seen that results from *P*–*T* axes are

https://doi.org/10.1017/S0016756802006489 Published online by Cambridge University Press

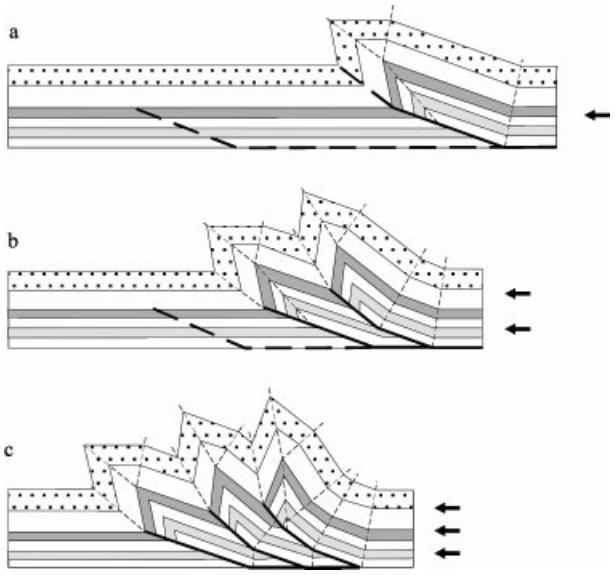

Figure 8. Geometric relationships and development of ramp anticlines in a leading thrust system (Mitra, 1986).

approximately the same. Consequently, the results derived from the *P–T* axes method, which is obtained by a computer program, are acceptable for us for the following calculations and interpretations.

5. Discussion

As a result of the determination of palaeostress directions of thrust faults (results of the *P–T* method), we have calculated differential ratios between stress directions on 49 selected faults. At the end of the section, the formation and the palaeostress distribution of normal and strike-slip-oblique thrust faults will be discussed.

Figure 12a represents the distributions of the ϕ values of 49 selected thrust faults. We calculated the stress ratio according to each individual fault within one known principal stress orientation. The stress ratio is computed by using the $\phi = 1 - (\tan\theta_\sigma/\tan\theta_n)$ formula of Ramsey & Lisle (2000). The ϕ values are increasing incrementally to 0.6 and give a peak point there. Thereafter, a drastic decrease occurs in the ϕ values between 0.6 and 0.8. Finally, ϕ values greatly increase again after 0.8 and peak between 0.9 and 1.0. Normally, a Gaussian-type curve would be expected for the data that occurred in the monophase deformation. The second part of the diagram (over $\phi > 0.8$), however, does not exhibit a similar curvature to the first one (under $\phi < 0.8$). Two factors can cause these changes: (a) the stress field was changed during formation of the faults that have the ϕ values greater than 0.8, and (b) stress ratios were changed during formation of the faults that have ϕ values more than 0.8. Considering the result of these changes we divided the data comprising 49 faults into two sets: (set-1) data that have ϕ values more than 0.8 and (set-2) data that have ϕ values less than 0.8. Figure 12b,c shows the set-1 and set-2 fault planes and corresponding striations. For both sets, palaeostress directions have been recalculated by the *P–T* axes method. Comparison of the stress fields of both sets reveals that there are no large differences in the stress field between set-1 and set-2 faults (Fig. 12b,c). This result allowed us to consider the second possibility, illustrated in (b). If the stress ratio has changed, it can be derived from the equation defined as $\phi = (\sigma1-\sigma2)/(\sigma1-\sigma3)$ (Ramsey & Lisle, 2000) that $\sigma2$ should have closer values to $\sigma3$. It means that $\sigma1 >> \sigma2 \cong \sigma3$.

Finally, we calculated deviation amounts between predicted shear direction (τ) that are obtained by applying ϕ values selected from Figure 12a ($\phi = 0.4$, 0.5, 0.6, and 0.9 respectively) on the stress field given in Figure 10a and the observed slip lineations (L) (Fig. 12d, e, f, g). As a result of the calculation it is seen that the angular misfit (d) has the lowest average value when ϕ is selected as 0.5. For other ϕ values, d is higher. In this study, we accepted that the average ϕ value for the entire data set (49 faults) is 0.5. General distribution of the ϕ values shows a very wide range but peak points occur at 0.5–0.6 and 0.8–1.0. The second peak has been discussed and interpreted in the previous paragraph. For the first peak (0.5–0.6), all of the σ values can be considered as different from each other ($\sigma1 > \sigma2 > \sigma3$). The diagrams of differential stress ratios have been interpreted by several authors (Flinn, 1962; Aleksandrowski, 1985; Lisle, 1989; Angelier, 1990; Delvaux *et al.* 1995; Srivastava, Lisle & Vandycke, 1995; Ramsey & Lisle, 2000). The first interpretation was done by Flinn (1962); the Flinn diagram can be divided into constrictional ($0.0 < \phi < 0.5$), plane ($\phi = 0.5$), and flattening ($0.5 < \phi < 1.0$) types of stress state (Lisle, 1989; Srivastava, Lisle & Vandycke, 1995). Stress ratios have been indicated as radial ($\phi = 0.1$), pure ($\phi = 0.5$), and strike-slip ($\phi = 0.9$) using the stress ratio formula of Angelier (1990) ($R = (\sigma2-\sigma3)/(\sigma1-\sigma3)$, $\phi = 1 - R$) in Delvaux *et al.* (1995) for compressive types of stress regime. In this study, we used the equation given by Ramsey & Lisle (2000):

$$\phi = (\sigma1-\sigma2)/(\sigma1-\sigma3)$$

for the interpretation, and the equation

$$\phi = 1 - (\tan\theta_\sigma/\tan\theta_n)$$

for the calculation. In this paper, stress ratios are interpreted as axial extension stress state ($0.5 < \phi < 1.0$) and axial compression stress state ($0.0 < \phi < 0.5$).

The pattern and palaeostress orientation compiled from small-scale normal faults (Fig. 11b) are consistent with the pattern of thrust faults (Fig. 11a). A π-diagram of normal fault planes reflects a similar density point, 18°/330° (Fig. 9b). The distribution of poles to slickenlines of the normal faults is roughly NW–SE (Fig. 9d). The maximum density point is 75°/140°. For the formation of the normal faults, we

https://doi.org/10.1017/S0016756802006489 Published online by Cambridge University Press

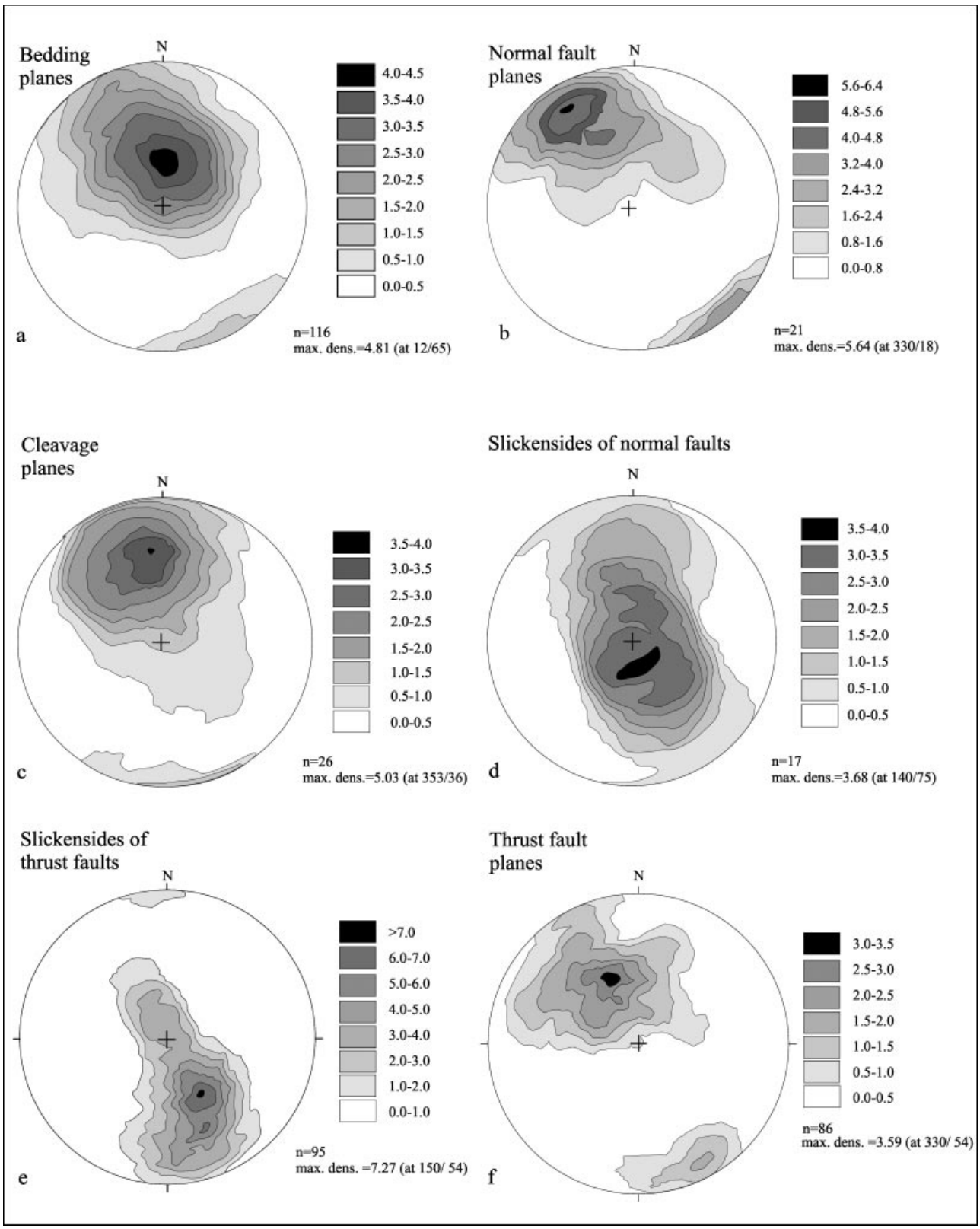

Figure 9. Lower-hemisphere, equal-area projections of structural data measured in the study area.

consider that fracture cleavages (disjunctive cleavages) rotate and transform into small domino-type normal faults (Fig. 5) by the mechanism of bedding-parallel shearing during folding. When a fold is simply sheared, on the normal limb of an overturned fold, normal faults can also develop because of extension of the normal limb that is exposed to positive shearing (Ramsey & Huber, 1989). Domino-type faults are bent towards the core of the fold where compression is dominant. Moreover, positive shearing of the normal

https://doi.org/10.1017/S0016756802006489 Published online by Cambridge University Press

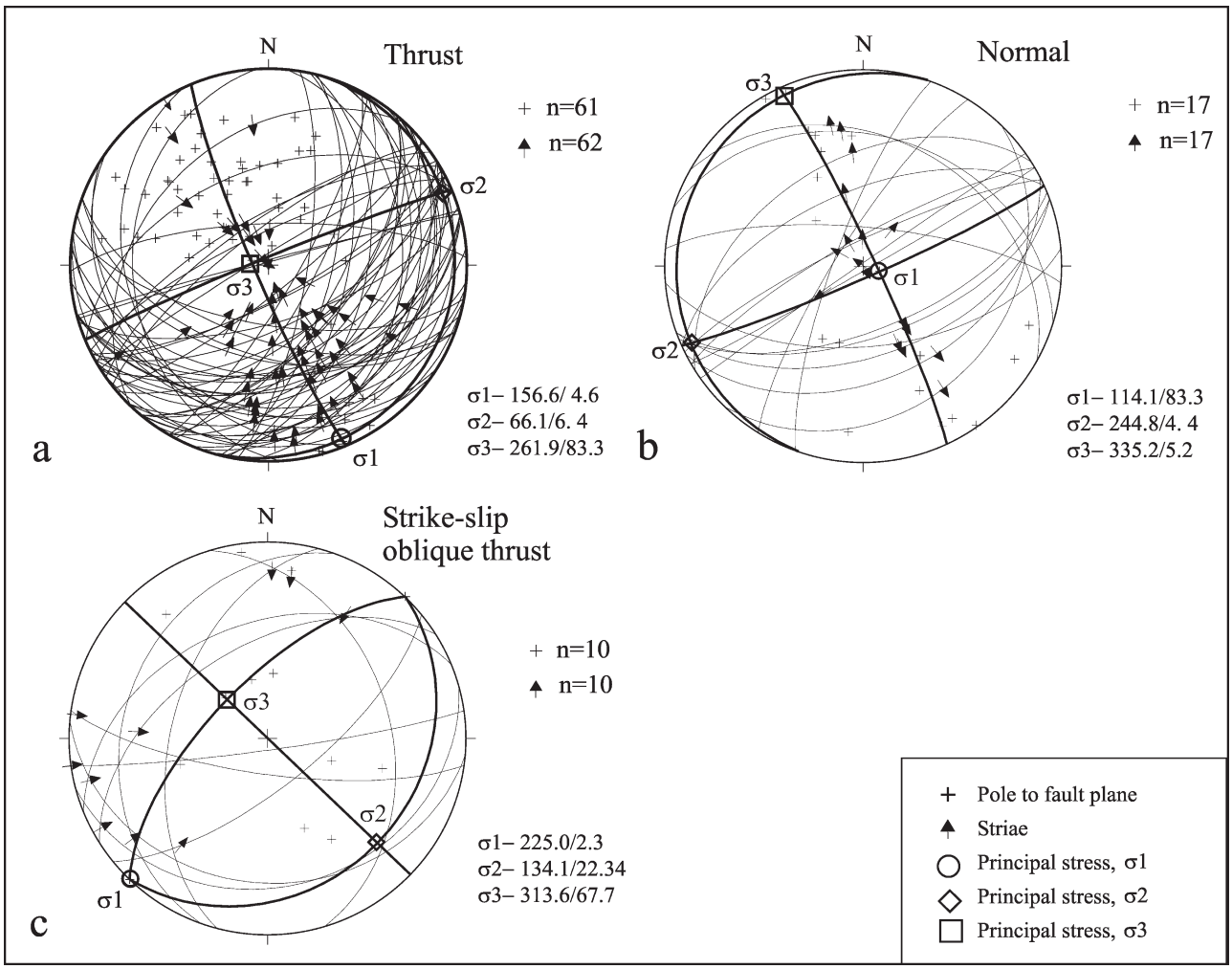

Figure 10. Lower-hemisphere, equal-area projections of different types of faults and palaeostress directions computed using the *P–T* method (Turner, 1953). (a) Thrust fault planes and corresponding striations; (b) normal fault planes and corresponding striations; (c) mainly strike-slip and oblique fault planes and corresponding striations. Great circle represents fault plane; cross and arrow represent plunge of striae and relative movement of the hanging wall.

limb causes small-scale normal faults to form by stretching of the normal limb (Fig. 5). In contrast to the thrust faults, normal faults are mainly S-dipping and the direction of movement is to the south. This supports the idea that the small-scale normal faults can develop on the normal limb of an overturned fold. Another possibility is that the older extensional structures were preserved, but there is no such observation in the study area.

Observed strike-slip and oblique thrust faults with a dominantly lateral component, as shown in Figure 10c, most probably developed under the compressional system. However, our measurements were not numerous enough to evaluate them satisfactorily. Furthermore, our field observations on curved slickenfibres support the idea that the thrust faults have transformed to oblique thrust and strike-slip faults over time. Such progressive transformation has been defined on curved slickenfibres in sheared rocks (Ramsey & Huber, 1989; Twiss & Gefell, 1990; Kusky, Bradley & Haeussler, 1997). This means that during later stages of deformation, the stress state and ratio changed and σ1 rotated towards a NE–SW direction (compare Fig. 10a and c). In addition, σ2 must be closer in value to σ3. As a result, our observations in the field and calculations on the ϕ values of the faults give sensible results for progressive deformation. In summary, it can be stated that a thrust regime changed progressively to an oblique thrust and then a strike-slip regime. The change to oblique thrusting was likely due to a change in the relative magnitudes of the principal stresses while the change to strike-slip faulting was likely triggered by a northeasterly rotation of the stress field.

The *P–T* axes and Angelier's M-pole girdle solution methods used in this study have been applied to structures that formed in different regions and tectonic regimes. Firstly, the *P–T* axes method was used for determining the principal axes from calcite twins by Turner (1953). Pfiffner & Burkhard (1987) discussed

https://doi.org/10.1017/S0016756802006489 Published online by Cambridge University Press

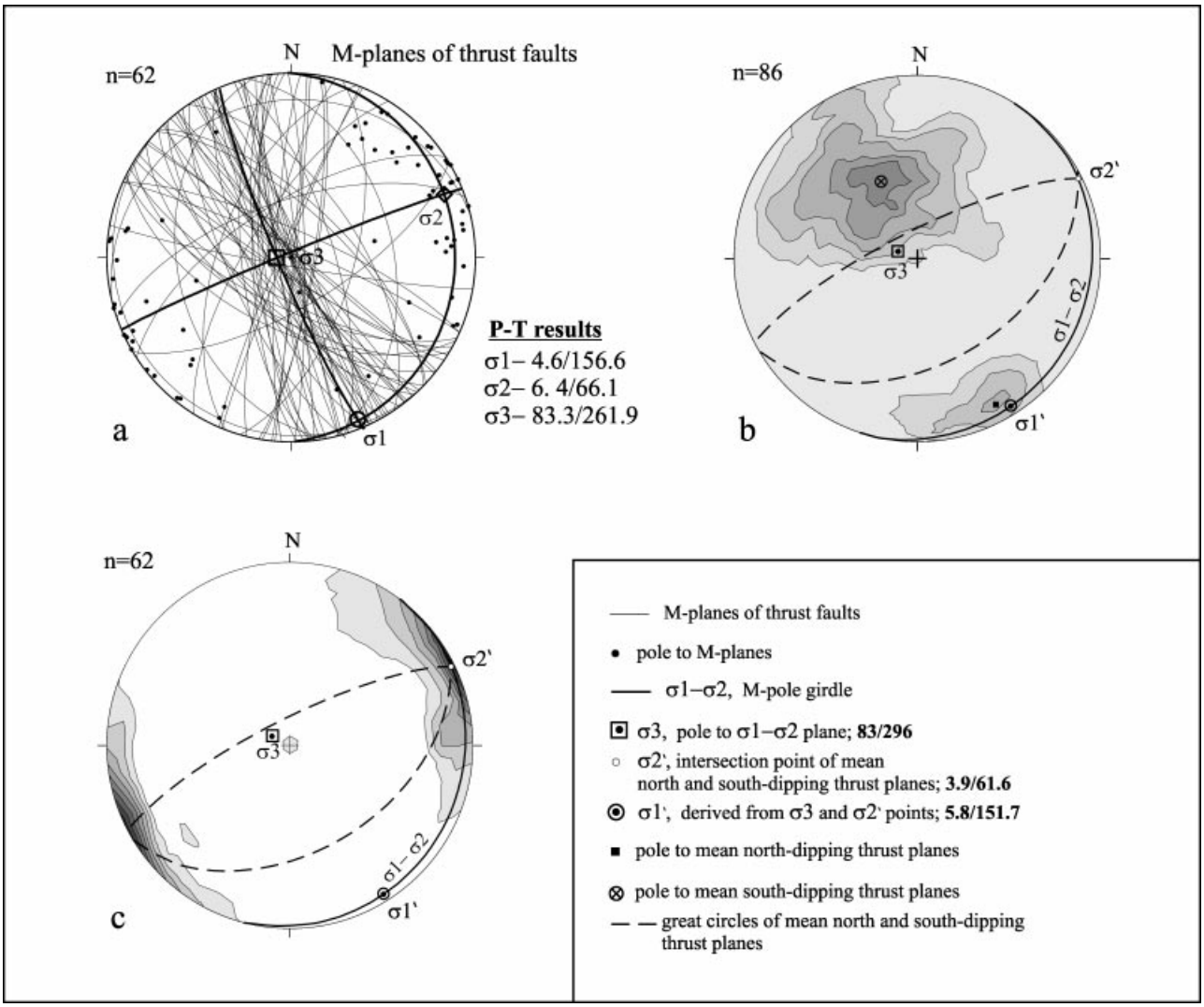

Figure 11. Lower-hemisphere, equal-area projections of (a) M-plane distribution of thrust faults and palaeostress results of *P–T* method; (b) density diagram of M-poles, M-pole girdle (σ1 and σ2 girdle), and pole to M-pole girdle (σ3); (c) density distribution of all thrust faults (Fig. 9f) and derived mean S- and N-dipping great circles of thrust faults. σ2′ is the intersection point of mean S- and N-dipping thrust faults (see text for details). σ1′ is the palaeostress direction that is derived from σ2′ and σ3 points (normal to the σ2′ and σ3 great circle).

applicability of the *P–T* axes and the right-dihedra and -trihedra methods to obtain palaeostress directions from fault, twin and earthquake data. Aleksandrowski (1985) compared Angelier's (1979, 1984) M-pole girdle method with Arthaud's (1969) M-plane solution and applied the methods to the region of Mt Babia Gòre of the Magura nappe in the Flysch Carpathians. Consequently, Aleksandrowski (1985) has shown two-stress state and relative rates of the principal stress directions of two different compressional episodes and interpreted development of separate fold and joint systems using these palaeostress directions.

Srivastava, Lisle & Vandycke (1995) also used *P–T* axes, right-dihedra and -trihedra, and numerical methods (direct inversion and four-dimensional exploration methods: Angelier, 1990) to establish the palaeostress directions and relationships of their relative rates. Especially ductile shear zones reveal that σ1 and σ2 are sub-horizontal and σ3 is approximately vertical, which defines the tectonic regime of compressive thrust that represents an analogue of our study in terms of the positions of principal stress directions.

In addition, many researchers have used the methods of *P–T* axes, Angelier's M-pole girdle, and right-dihedra and -trihedra to determine palaeostress directions that formed in different tectonic settings, and relative rates between them (e.g. Angelier, 1984, 1990; Marrett & Allmendinger, 1990; Delvaux *et al.* 1995; Huerta & Rodgers, 1996).

6. Conclusions

The units representing the opening of the Black Sea were squeezed after the closing of the Neotethyan Ocean to the south, and were imbricated by the N-vergent thrust faults during the Late Eocene–Early Miocene

https://doi.org/10.1017/S0016756802006489 Published online by Cambridge University Press

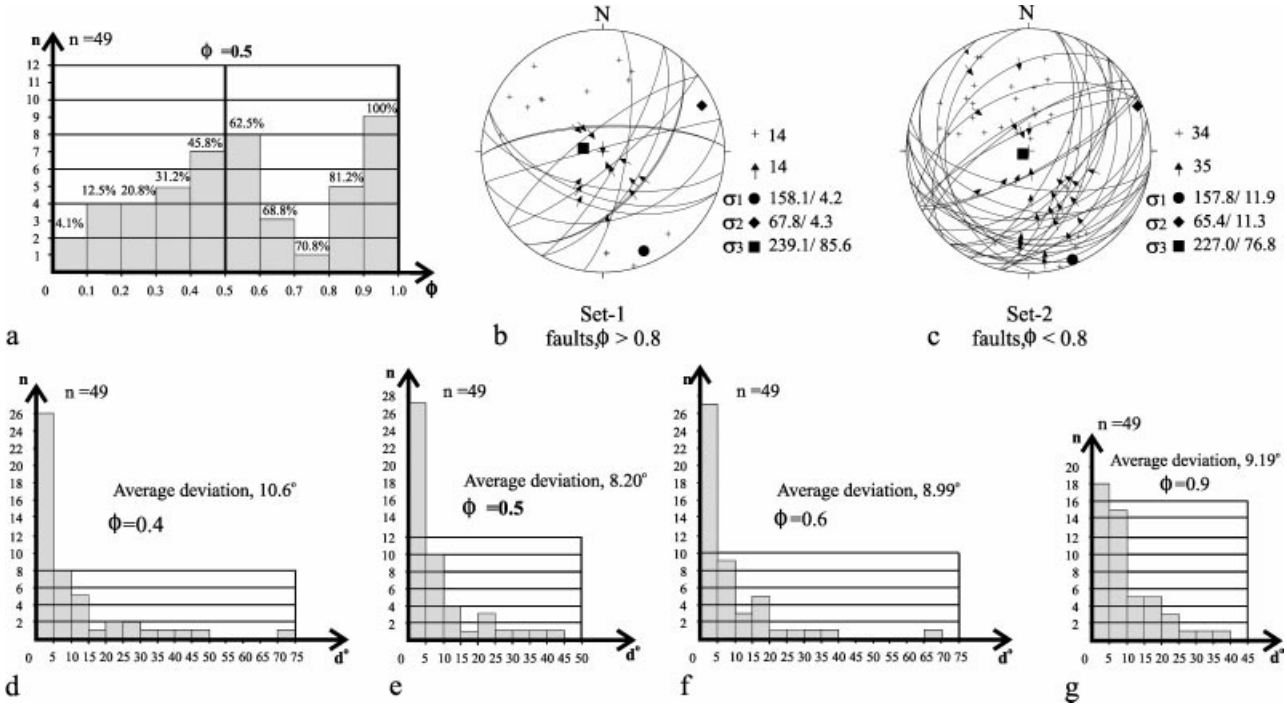

Figure 12. (a) ϕ value distribution of 49 selected thrust faults, which are computed according to the palaeostress state given in Figure 11a; (b) distribution of set-1 faults ($\phi > 0.8$) and palaeostress directions (computed using *P–T* method); (c) distribution of set-2 faults ($\phi < 0.8$) and palaeostress directions (computed using *P–T* method) (great circle represents fault plane; cross and arrow represent plunge of striae and relative movement of the hanging wall); (d, e, f, g) deviation (in degrees) of theoretical shear directions with computed ϕ values of 0.4, 0.5, 0.6 and 0.9 respectively and observed lineations ($d° = |\tau – L|$). n: number of faults, $\phi = (\sigma1–\sigma2)/(\sigma1–\sigma3)$ (Ramsey & Lisle, 2000). σ1, σ2 and σ3 are the palaeostress directions computed using the *P–T* method (Turner, 1953).

period. This compression started soon after the deposition of the Cambu Formation and affected Middle Eocene and older units of the study area.

The Upper Cretaceous units are absent in the southern parts of the study area and their thickness increases close to the thrust faults; thus it is considered that some of the normal faults belonging to a previous extensional system were reworked as thrust faults (inversion tectonics). Kinematically, it is possible that antithetic normal faults facing southward could be reworked by thrusts.

The results of palaeostress analyses from the thrust faults reveal sub-horizontal orientations of the σ1 and σ2 axes, suggesting the development of these faults in a compressive and thrust tectonic regime. Calculated palaeostress directions of thrust faults shown in Figure 11a are 4.6°/156.6 ° for σ1, 6.4°/66.1° for σ2 and 83.2°/261.9° for σ3. The vergence interpreted from Figure 9 is between N7°W and N30°W. Evaluation of structural characteristics of the study area implies that the tectonic style of the area is a foreland fold and thrust belt. The general structural style of the area is a leading imbricated thrust system (Fig. 7). The examples of both macro- and meso-structures developed here are analogous to those in the Canadian Rockies (Dahlstrom, 1969) and the Appalachians (Harris & Milici, 1977).

The comparison of stress diagrams of thrust and normal faults show that the locations of the stress axes of each are approximately equivalent. It is considered that all extensional structures in the study area, which are small-scale and shallow, have developed under a compressional system together with thrust faults. The extensional faults are localized within the limbs of larger compressional folds.

In the southern part of the area where basement (older) rocks are involved, deformation is not penetrative, in contrast to the northern part of the area. Towards the north, the intensity of deformation increases. The study area is suggested to have been compressed more than 50% with this shortening being accommodated by the fold style and the thrusts (Şengör, 1995; Akçiz *et al.* 1997). The decrease of dip angles of the fault planes towards the north suggests that the faults may be connected to a detachment fault at depth. If the idea of such a detachment surface within the Lower Cretaceous unit (Şengör, 1995) is relevant, such a surface should be at least 5 km deep in the offshore region. Average thickness of the overburden on the Lower Cretaceous unit is about 2.5 km, and if the 50% shortening is taken into account, the Lower Cretaceous unit should be at least 5 km deep.

After the collision of the Anatolian and Arabian plates 11 Ma ago, escape tectonics started to affect the Anatolian plate. The most important structure of this escape regime, the North Anatolian Transform Fault (Şengör, 1979; Barka, 1992), lies along the south of the

https://doi.org/10.1017/S0016756802006489 Published online by Cambridge University Press

Pontides. The effect of this young and still-active strike-slip regime to the Western Pontides is a matter of debate. The lack of sedimentary rocks younger than the Oligocene in the east of the Adapazarı and Karasu line (Fig. 1), except within some depressions to the south of the Pontides, may be attributed to the continuing uplift of the Black Sea Mountains since the Oligocene. The deeply eroded mountainous morphology of the area also indicates an active uplift. In addition, a reverse fault solution has been determined for the 1968 Bartın earthquake (Taymaz & Tan, 1999). All these data may be interpreted to mean that the eastern part of the Western Pontides it is still under the effect of a compressional regime.

Acknowledgements. We thank the Turkish Petroleum Co. who supported this study. Aral Okay, Boris Natalin and Serdar Akyüz of Istanbul Technical University carefully read and improved the manuscript. We also thank Ufuk Tarı and Aynur Dikbaş of Istanbul Technical University for helping us produce the digital map of the study area and the figures of the manuscript. We thank Jordan Muller and an anonymous referee for their valuable contributions.

References

Abdüsselamoğlu, M. Ş. 1977. *The Palaeozoic and Mesozoic in the Gebze region*. Explanatory text and excursion guide book. 4th Colloqium on the Geology of the Aegean Region, Excursion 4: Western Anatolia and Thrace. Istanbul Technical University, Faculty of Mines, 16 pp.

Akçız, S., Yilmaz, R., Tüysüz, O. & Şengör, A. M. C. 1997. Backthrusting-related fold and thrust belt in the Central Pontides. *Geological Society of America 1997 Annual Meeting, October 20–23, Salt Lake City, Utah, Abstracts with Programs*, A–47.

Akman, A. Ü. 1992. Karadeniz çevresi havzalarının açılış mekanizmaları ve yaşı, KB Türkiye. *9th Petroleum Congress and Exhibition of Türkiye, Proceedings Geology, Turkish Association of Petroleum Geologists, Hilton International, Ankara*, 307–19.

Akyol, Z., Arpat, E., Erdoğan, B., Göğer, E., Şaroğlu, F., Şentürk, İ., Tütüncü, K., & Uysal, Ş. 1974. *Geologic Map of Turkey Quadrangle Series, Zonguldak E29a, E29b, E29c, E29d, Kastamonu E30a, E30d.* Mineral Research and Exploration Institute of Turkey, Ankara.

Aleksandrowski, P. 1985. Graphical determination of principal stress direction for slickenside lineation populations: an attempt to modify Arthaud's method. *Journal of Structural Geology* **7**(1), 73–85.

Alişan, C. & Derman, A. S. 1995. The First Palynological Age, Sedimentological and Stratigraphic Data for the Çakraz Group (Triassic), Western Black Sea. In *Proceedings of the International Symposium on the Geology of the Black Sea Region* (eds A. Erler, T. Ercan, E. Bingöl and S. Örçen), pp. 93–8. General Directorate of Mineral Research and Exploration and Chamber of Geological Engineers, Ankara, Turkey.

Angelier, J. 1979. Determination of the mean principle directions of stress for a given fault population. *Tectonophysics* **56**, 17–26.

Angelier, J. 1984. Tectonic analysis of fault-slip data set. *Journal of Geophysical Research* **89**, 5835–48.

Angelier, J. 1990. Inversion of field data in fault tectonics to obtain the regional stress – III. A new rapid direct inversion method by analytical means. *Geophysical Journal International* **103**, 363–76.

Arthaud, F. 1969. Methode de determination graphique des directions de raccourcissement, d'allongement et intermediaire d'une population de failles. *Bulletin Geological Sociéte de France* **7**, Ser. 11, 729–37.

Barka, A. A. 1992. The North Anatolian Fault. *Annales Tectonicae* **6**, 164–95.

Berger, P. & Johnson, A. M. 1980. First order analysis of deformation of a thrust sheet moving over a ramp. *Tectonophysics* **70**, 9–24.

Canca, N. 1994. *1:100.000 ölçekli Türkiye Batı Karadeniz Taşkömürü Havzası Jeoloji haritaları.* General Directorate of Mineral Research and Exploration, Scientific Publications Division, Ankara, 10 pp.

Dahlstrom, C. D. A. 1969. Balanced cross sections. *Canadian Journal of Earth Science* **6**, 743–57.

Delvaux, D., Moeys, R., Stapel, G., Melnikov, A. & Ermikov, V. 1995. Palaeostress reconstructions and geodynamics of the Baikal region, Central Asia, Part I. Paleozoic and Mesozoic pre-rift evolution. *Tectonophysics* **252**, 61–101.

Derman, A., S. Alişan, C. & Özçelik, Y. 1995. Himmetpaşa Formation: New palinological age data and significance. In *Proceedings of the International Symposium on the Geology of the Black Sea Region* (eds A. Erler, T. Ercan, E. Bingöl, and S. Örçen), pp. 99–104. General Directorate of Mineral Research and Exploration and Chamber of Geological Engineers, Ankara, Turkey.

Finetti, I., Bricchi, G., Del Ben, A., Pipan, M. & Xuan, Z. 1988. Geophysical study of the Black Sea area. *Bulletino Geofisica Teorica ed Applicata. Monograph on the Black Sea* **30**(117–118), 197–324.

Flinn, D. 1962. On folding during three-dimensional progressive deformation. *Quarterly Journal of the Geological Society of London* **118**, 385–428.

Görür, N. 1988. Timing of opening of the Black Sea basin. *Tectonophysics* **14**, 247–62.

Görür, N. 1997. Cretaceous syn- to post-rift sedimentation on the southern continental margin of the Western Black Sea Basin. In *Regional and Petroleum Geology of the Black Sea and surrounding region* (ed. A. G. Robinson), pp. 227–40. American Association of Petroleum Geologists, Memoir no. 68.

Görür, N., Monod, O., Okay, A. I., Şengör, A. M. C., Tüysüz, O., Yiğitbaş, E., Sakinç, M. & Akkök, R. 1997. Palaeogeographic and tectonic position of the Carboniferous rocks of the western Pontides (Turkey) in frame of the Variscan belt. *Bulletin Société Géologique de France* **168**(2), 197–205.

Görür, N., Okay, A. I., Tüysüz, O., Yiğitbaş, E. & Akkök, R. 1995. Istanbul-Zonguldak Paleozoyik istifinin Paleocoğrafik ve tektonik konumu. In *Zonguldak Havzası Araştırma Kuyuları-I: Kozlu-K20/G* (eds M. N. Yalçın and G. Gürdal), pp. 27–43. TUBITAK, Marmara Research Center Special Publication, Gebze, Kocaeli, Turkey.

Görür, N., Şengör, A. M. C., Akkök, R. & Yilmaz, Y. 1983. Pontidler'de Neo-Tetis'in kuzey kolunun açılmasına ilişkin sedimentolojik veriler. *Türkiye Jeoloji Kurumu Bülteni* **26**(1), 11–20.

Görür, N. & Tüysüz, O. 1997. Petroleum geology of southern continental margin of the Black Sea. In *Regional*

and Petroleum Geology of the Black Sea and surrounding region (ed. A. G Robinson), pp. 241–54. American Association of Petroleum Geologists, Memoir no. 68.

Görür, N., Tüysüz, O., Aykol, A., Sakinç, M., Yiğitbaş, E. & Akkök, R. 1993. Cretaceous red pelagic carbonates of northern Turkey: Their place in the opening history of the Black Sea. *Eclogae geologicae Helvetica* **86**(3), 819–38.

Harris, L. D. & Milici, R. C. 1977. Characteristics of thin-skinned style of deformation in the southern Appalachians and potential hydrocarbon traps. *USGS Professional Paper* **1018**, 1–40.

Huerta, A. D. & Rodgers, D. W. 1996. Kinematic and dynamic analysis of a low-angled strike-slip fault: the lake Creek Fault of south-central Idaho. *Journal of Structural Geology* **18**, 585–93.

Johannes, D. 2000. *StereoNet Version 2.46*. Shareware, Copyrighted Software.

Kusky, T. M., Bradley, D. G. & Haeussler, P. 1997. Progressive deformation of the Chugach accretionary complex, Alaska, during a Paleogene ridge–trench encounter. *Journal of Structural Geology* **19**, 139–57.

Lisle, R. J. 1989. Palaeostress analysis from sheared dike sets. *Bulletin of the Geological Society of America* **101**, 968–72.

Marrett, R. & Allmendinger, R. W. 1990. Kinematic analysis of fault-slip data. *Journal of Structural Geology* **12**, 973–86.

Mitra, S. 1986. Duplex structures and imbricated thrust systems: Geometry, structural position and hydrocarbon potential. *American Association of Petroleum Geologists Bulletin* **70**, 1087–1112.

Mitra, S. 1990. Fault-propagation folds: geometry, kinematic evolution and hydrocarbon traps. *American Association of Petroleum Geologists Bulletin* **74**, 921–45.

Nickelsen, N. P. 1963. Fold patterns and continuous deformation mechanisms of the central Pennsylvania folded Appalachians. In *Guidebook to tectonics and Cambro-Ordovician Stratigraphy, central Appalachians of Pennsylvania*, pp. 13–29. Pittsburgh Geological Society.

Okay, A. İ., Şengör, A. M. C. & Görür, N. 1994. Kinematic history of the opening of the Black Sea and its effect on the surrounding regions. *Geology* **22**, 267–70.

Okay, A. İ., Tansel, I. & Tüysüz, O. 2001. Obduction, subduction and collision as reflected in the Upper Cretaceous–Palaogene sedimentary record of western Turkey. *Geological Magazine* **138**, 117–42.

Okay, A. İ. & Tüysüz, O. 1999. Tethyan Sutures of northern Turkey. In *The Mediterranean Basins: Tertiary Extension within the Alpine Orogen* (eds B. Durand, L. Jolivet, F. Hovarth and M. Séranne), pp. 475–515. Geological Society of London, Special Publication no. 156.

Passchier, C. W. & Trouw, R. A. J. 1996. *Micro-tectonics*. Springer-Verlag, 289 pp.

Pfiffner, O. A. & Burkhard, M. 1987. Determination of paleo-stress axes from fault, twin and earthquake data. *Annales Tectonicae* **I**, 48–57.

Ramsey, J. G. & Huber, M. I. 1989. *The Techniques of Modern Structural Geology*, *Volume 1: Strain Analysis*. London: Academic Press Limited, 307 pp.

Ramsey, J. G. & Lisle, R. J. 2000. *The Techniques of Modern Structural Geology, Volume 3: Application of continuum mechanics in structural geology*. London: Academic Press Limited, 1061 pp.

Şengör, A. M. C. 1979. The North Anatolian transform fault: its age, offset and tectonic significance. *Journal of the Geological Society, London* **136**, 269–82.

Şengör, A. M. C. 1995. The Large Tectonic Framework of the Zonguldak Coal Basin in Northern Turkey: An Outsider's View. In *Zonguldak Havzası Araştırma Kuyuları-I: Kozlu-K20/G* (eds M. N. Yalçın. and G. Gürdal), pp. 1–26. TUBITAK, Marmara Research Center Special Publication, Gebze, Kocaeli, Turkey.

Şengör, A. M. C. & Yilmaz, Y. 1981. Tethyan evolution of Turkey: A plate tectonic approach. *Tectonophysics* **75**, 181–241.

Srivastava, D. C., Lisle R. J. & Vandycke, S. 1995. Shear zones as a new type of palaeostress indicator. *Journal of Structural Geology* **17**, 663–76.

Suppe, J. & Medwedeff, D. A. 1984. Fault-propagation folding. *Geological Society of America Abstracts with Programs* **16**, 670.

Suppe, J. & Medwedeff, D. A. 1990. Geometry and kinematics of fault-propagation folding. *Eclogae geologicae Helvetica* **83**, 409–54.

Suppe, J. 1983. Geometry and kinematics of fault-bend folding. *American Journal of Science* **283**, 684–721.

Taymaz, T. & Tan, O. 1999. Source parameters of September 3, 1968 Bartın (SW-Black Sea) and October 5, 1977 Kurşunlu (NAF) earthquakes from inversion of teleseismic body-waveforms. *22nd General Assembly of International Union of Geodesy and Geophysics (IUGG). IASPEI-Symposia: Seismotectonics of Eurasia ST2/E/13-A5. Abstracts Book-A,* p. A-169. The University of Birmingham, UK, July 19–30, 1999.

Turner, F. J. 1953. Nature and dynamic interpretation of deformation lamellae in calcite of three marbles. *American Journal of Science* **251**, 276–98.

Tüysüz, O. 1990. Tectonic evolution of a part of the Tethyside orogenic collage: The Kargı massif, Northern Turkey. *Tectonics* **9**, 141–60.

Tüysüz, O. 1993. Karadeniz'den Orta Anadolu'ya Bir Jeotravers: Kuzey Neo-Tetis'in Tektonik Evrimi. *Turkish Association of Petroleum Geologists Bulletin* **5**(1), 1–33.

Tüysüz, O. 1999. Geology of the Cretaceous sedimentary basins of the Western Pontides. *Geological Journal* **34**, 75–93.

Tüysüz, O., Dellaloğlu, A. A. & Terzioğlu, N. 1995. A magmatic belt within the Neo-Tethyan suture zone and its role in the tectonic evolution of Northern Turkey. *Tectonophysics* **243**, 173–91.

Tüysüz, O., Keskin, M. & Sunal, G. 1999. The opening of Western Black Sea basin. *Türkiye Denizlerinde Jeoloji-Jeofizik araştırmaları. Workshop V, Extended Abstracts. General Directorate of Mineral Research and Exploration, Ankara*, 62–4.

Tüysüz, O., Yilmaz, Y., Yiğitbaş, E. & Serdar, H. S. 1990. Orta Pontidlerde Üst Jura-Alt Kretase stratigrafisi ve anlamı. *8th Petroleum Congress of Turkey, Geology Proceedings, Turkish Association of Petroleum Geologists, Chamber of Petroleum Engineers, Ankara*, 340–50.

Twiss, R. J. & Gefell, M. J. 1990. Curved slickenfibers: a new brittle shear sense indicator with application to a sheared serpentinite. *Journal of Structural Geology* **12**, 471–81.

Yiğitbaş, E., Elmas, A. & Yilmaz, Y. 1999. Pre-Cenozoic tectonostratigraphic components of the Western Pontides and their geological evolution. *Geological Journal* **34**, 55–74.